J Mater Sci (2017) 52:138–144

Aspect ratio effects on the serration dynamics of a Zr-based bulk metallic glass

Z. F. Yao[1], J. C. Qiao[1,*], Y. Liu[2], J. M. Pelletier[3], and Y. Yao[1,*]

[1] School of Mechanics, Civil Engineering and Architecture, Northwestern Polytechnical University, Xi'an 710072, People's Republic of China
[2] Department of Earth Sciences, Debye Institute for Nanomaterials Science, Utrecht University, Princetonplein 5, 3584 Utrecht, The Netherlands
[3] Université de Lyon, MATEIS, UMR CNRS5510, Bat. B. Pascal, INSA-Lyon, 69621 Villeurbanne Cedex, France

Received: 18 June 2016
Accepted: 18 August 2016
Published online:
24 August 2016

ABSTRACT

Based on the constant strain rate compressive experiments to a Zr-based bulk metallic glass, the aspect ratio effects on the statistical properties of serration is systematically investigated. In the plastic deformation state, as the aspect ratio decreases, the stress drop magnitude increases dramatically and the reloading time in one serration event increases significantly. Moreover, distribution of the elastic energy density of each serration event is predicted, which obeys the squared exponential decay law. The size effect law is adopted to describe the serration dynamic-related parametric variation with different aspect ratios. It is noted that the scaling exponent reduces with the increase of the aspect ratio. In general, the effect of aspect ratio on the serration flow could be explained by the shear-band stability index.

Introduction

The mechanical properties of bulk metallic glasses (BMGs) have been studied extensively due to their excellent mechanical properties, such as high strength, large elastic limit, and other unique physical properties [1–5]. However, most of the BMGs fail in a brittle or quasi-brittle manner with limited ductility at room temperature, which severely restricts their potential engineering applications [1–5]. The plastic deformation of BMGs is strongly related to the formation of highly localized shear bands [1–4]. The serrations during compression on the stress–strain curve correspond with the shear-band formation directly [6–9]. Serrated flows are known as repeated yielding of BMGs during plastic deformation, which is associated with the shear-band nucleation and propagation [10]. There has been a great amount of attempts to explain the mechanism during plastic deformation experimentally and theoretically [11–28]. Generally, material compositions, strain rate, temperature, mean stress drop magnitude (burst size), elastic energy density, and duration time could affect the serration characteristics of the BMGs.

Recently, the micro-alloying effect on the plasticity and serration behavior was studied [29]. It reveals

Address correspondence to E-mail: qjczy@hotmail.com; qjczy@nwpu.edu.cn; yaoy@nwpu.edu.cn; yaooay@gmail.com

DOI 10.1007/s10853-016-0316-7

that the statistical parameters of serration behavior changes with subtle variation of the composition. Based on the spatial temporal dynamic model and squared exponential decay function, the self-organized critical (SOC) behavior could be predicted [30–32]. Moreover, nanoindentation test [33, 34] was also conducted to study the serrated behavior, which shows that slower indentation velocity assists the serration, and vice versa. The relationship between serrations and shear bands nucleation/propagation dynamics was studied extensively [35–46]. The previous studies reveal that the BMGs can exhibit large inelastic deformation under confinement [42, 43], especially when the aspect ratio is lower than one. The plasticity with lower aspect ratio is due to the shear-band nucleation and propagation [40]. Moreover, considering the sample size and machine stiffness, the serration flow could be characterized by the shear-band instability index, which is proportional to the sample size and inversely to the machine stiffness [47].

In the present work, the influence of sample aspect ratio on the serration dynamics was investigated combining with statistical analysis. The characteristic duration time, burst size, and distribution of the elastic energy density in the serration events under different aspect ratios were studied and discussed. The size effect law proposed by Bažant [48, 49] shows that size effect is induced by the mismatch between the required energy to propagate shear band and the internal energy released. This model was adopted to describe variation of the parameters such as plastic strain, yield stress, scaling exponent, and the average elastic energy density. The $Zr_{40}Ti_{25}Cu_8Be_{27}$ BMG was selected in the current research due to its good glass formation ability and thermal properties [50]. Good plasticity at room temperature was observed in the compression tests.

Experimental procedures

The ingots of master alloy with nominal composition of $Zr_{40}Ti_{25}Cu_8Be_{27}$ (at.%) BMG were fabricated. The rod samples (3 mm in diameter, 70 mm in length) were obtained by water-cooled copper mold suction casting. The amorphous nature of these rods was confirmed by X-ray diffraction and differential scanning calorimetry. The test samples were obtained from the lower half part of the as-cast rods and subsequently prepared with nominal aspect ratios of 6:3, 5:3, 4:3, and 3:3, respectively. Both ends of the sample were carefully grinded parallel to each other within the accuracy of 20 μm and perpendicular to the longitudinal axis. Uniaxial compression tests were conducted with a constant strain rate of $8 \times 10^{-5}\ s^{-1}$ at room temperature. At least three samples with the same aspect ratio were tested to ensure the reliability of results.

Results and discussion

The compressive stress–strain curves of the BMG exhibit serrated flow behavior after yielding under different aspect ratios, as shown in Fig. 1a. Mechanical and statistical properties of the BMG are listed in Table 1. The serration event is known as cyclic yielding of the BMG in the plastic steady-state deformation, which is characterized by the cycles of a sudden stress drop and followed by the reloading, as shown in Fig. 1b. The elastic energy density ($\Delta\delta$) is defined as $\Delta\sigma\Delta\varepsilon/2$, where $\Delta\sigma$ and $\Delta\varepsilon$ are the range of stress and strain in one serration event [31, 32]. The serrated flow is related to the shear banding [40]. Scanning electron microscopes (SEM) images were recorded in 20 kV with a beam current of 2.4 nA on a Focus ion beam scanning electron microscopes system of FEI Nova Nanolab 600, installed at Utrecht University of the Netherlands. Figure 1c–f shows the SEM images of different aspect ratios; only one dominant shear band is shown in Fig. 1c, while several dominant shear bands are shown in Fig. 1d, e. Meanwhile some secondary shear bands are located away from the fracture surface, which are randomly generated. With the aspect ratio reducing to 3/3, profuse shear bands can be observed which are caused by the geometry constraints, as shown in Fig. 1f. Under lower aspect ratio, higher density of the shear bands occurred, which is induced by the geometry constraints [42, 43]. The dominant shear bands form and propagate continually, and eventually cause fracture under non-geometry constraints. As the aspect ratio reduces continuously, the fracture mode transits from one dominant shear-band catastrophically fracture to the geometry constraints ductile fracture. In other words, it corresponds to the transition from chaotic (non-serration) to SOC behavior. As shear bands consume part of the energy, the large elastic energy density in one serration could be correlated to more than one shear band, which is consistent with the previous study [31, 32].

In the plastic steady state, the temporal dynamics of the serration events (Fig. 2) under different aspect ratios was investigated. Initially, the stress gradient |dσ/dt| curves within plastic stain range show that the time interval t_n between any two neighboring serrations is stochastic and inhomogeneous, which reveals that the serration flow events are lack of typical time scale [31]. In general, the serrated flow has clear and well-defined time scales [40]; however, the diffused shear bands caused disappear of characteristic time scale in the present study. This is the thread of time-free activity with the absence of the characteristic time in the BMG. Secondly, the elastic stress reloading time t_R is much larger than the stress drop time t_D, which represents that internal stress relaxation is much faster than the increase of external stress to reach a dynamic equilibrium, i.e., SOC state. In other words, the plastic deformation of BMGs should be considered within a non-equilibrium framework because the scale-free process is involved [31].

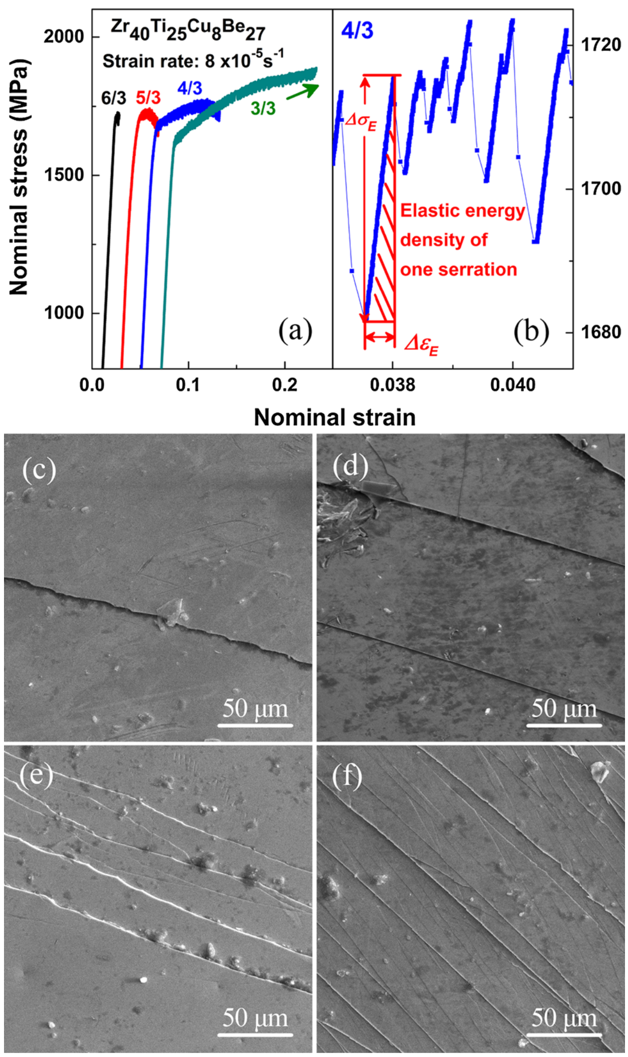

Figure 1 **a** Stress–strain curves of the $Zr_{40}Ti_{25}Cu_8Be_{27}$ BMG compressed under different aspect ratios. **b** Elastic energy density for one serration, the serration is extracted from the curve of aspect ratio 4/3. **c–f** SEM images for the shear bands morphology with various aspect ratios.

It should be noted that with the decrease of the aspect ratio, the value of t_R/t_D increases dramatically; it manifests that the serrated flow behavior is dependent on the aspect ratio in this BMG, which is consistent with previous research [42–45]. The average amplitudes of stress drop are 11, 20, 22, and 27 MPa, corresponding to aspect ratio of 6/3, 5/3, 4/3, and 3/3, respectively, which also accounts for the dependence of serrated flow behavior to the aspect ratio, as shown in Fig. 2.

To investigate the serration dynamics and its correlation with shear stability under different aspect ratios, statistical analysis of the elastic energy density was performed, as shown in Fig. 3. Under different aspect ratios, the values of δ_C changed because the shear band assists plastic deformation. It is shown that the cumulative probability distribution, $P(\geq\Delta\delta)$, is non-linear with respect to the value of $\Delta\delta$ [31]. Smaller values of $\Delta\delta$ follow a power-law distribution, which indicates that the serration flow has a SOC behavior. Meanwhile, the larger values of $\Delta\delta$ decrease exponentially in probability, and the chaotic dynamics starts to play a dominant role in the

Table 1 Fracture strain (ε_f), plastic strain (ε_p), Young's modulus (E), yield stress (σ_y), scaling exponent (β), normalization constant (A), and cut-off value for the elastic energy density (δ_C) of the $Zr_{40}Ti_{25}Cu_8Be_{27}$ BMG, where T_g = 578 K

Aspect ratio	ε_f	ε_p	E (GPa)	σ_y (MPa)	β	δ_C (J/m^3)	A
6/3	0.028	0.011	99.4	1690	0.18	8185	2.60
5/3	0.049	0.031	93.6	1685	0.40	12000	10.20
4/3	0.092	0.075	98.2	1670	0.26	11039	4.38
3/3	0.173 (not fracture)	0.156	97.6	1660	0.20	5614	3.04

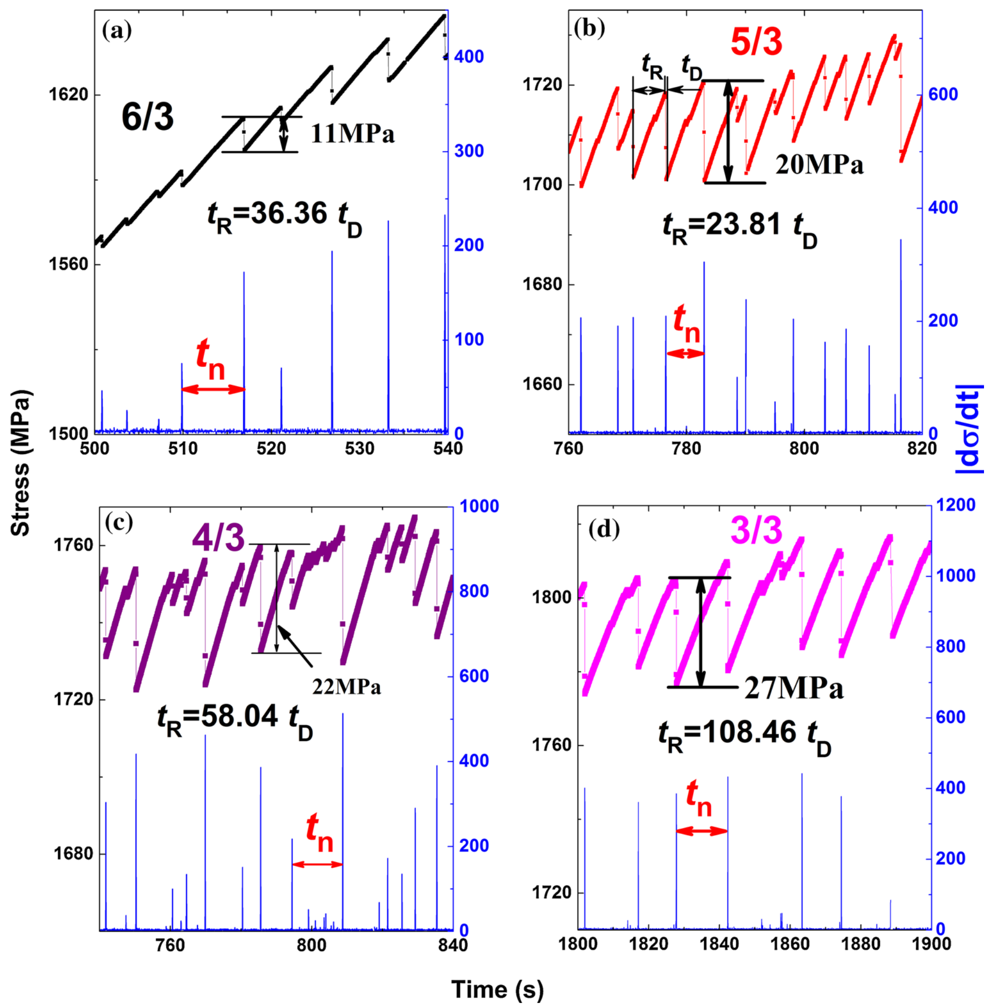

Figure 2 The stress–time and corresponding derivative of $|d\sigma/dt|$ versus time relation at different aspect ratios. t_R is the stress reloading time and t_D is the decreasing time.

deformation process [6, 11, 12]. These serration behaviors could be approximated by power-law distribution with a squared exponential decay function [31, 51]:

$$P(\geq \Delta\delta) = A\Delta\delta^{-\beta}\exp[-(\Delta\delta/\delta_C)^2], \quad (1)$$

where A is the a normalized constant, β is a scaling exponent, and δ_C represents the cut-off elastic energy density.

The fitting parameters of four different aspect ratios are listed in Table 1. The β value increases with higher variations of serration elastic energy density. It indicates that the β parameter reflects size evolution of the serration events, and larger β value represents fast shear bands propagation and eventually fractured, which is consistent with the experimental results. For lower aspect ratios, the effect of geometry constraint is pronounced and subsequently the shear-band propagation could be hindered by the pressure head. In addition, when the elastic energy density exceeds δ_C (cut-off value), the squared exponential decay factor comes into play.

The parameter δ_C is related to ductility of the BMGs, and with the aspect ratio being reduced, the ductility is increased with larger δ_C value. Therefore, the three parameters in Eq. (1) reflect a serration dynamics of the BMG. Han et al. [47] proposed a shear-band stability index, which is proportional to sample size and inversely proportional to machine stiffness, for the cylindrical samples:

$$S_{cr} = \pi ED/4RK_M, \quad (2)$$

where E is the Young's modulus, K_M is the testing machine stiffness, D is the sample diameter, R is the aspect (height-to-diameter) ratio. Below S_{cr}, the shear bands mobility is stable, and vice versa. In the present study, the values of E, D, K_M are constants, and therefore, S_{cr} is inversely related to R, i.e., when R reduces, S_{cr} increases simultaneously and enhances

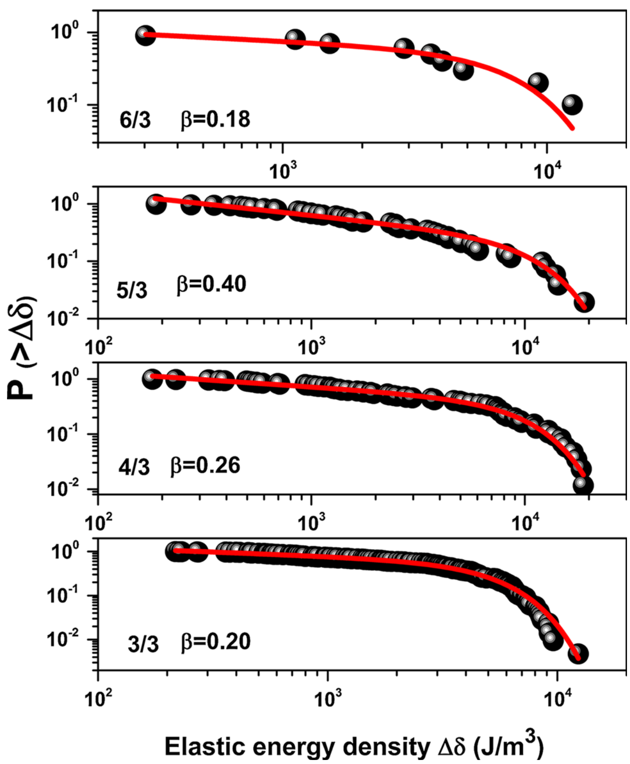

Figure 3 Cumulative probability distributions $P(>\Delta\delta)$ for the elastic energy densities of the four aspect ratios. The data points are experimentally measured from the compressive stress–strain curves. The *red solid lines* are fitted based on Eq. (1).

the shear-band stability, which is consistent with the experimental observations.

To further understand the aspect ratio effect on the serration dynamics of BMG, the size effect law [48, 49] was used to analyze the deformation process, which indicates that dissipation of the strain energy could be affected by the macroscopic geometry. Microscopic shear bands initiation and propagation are correlated with the macroscopic crack formation, and they are induced by the dissipation of strain energy. In other words, serration is a microscopic discontinuous energy dissipations process. The size effect could cause stress redistribution and dissipation of the storage energy, and subsequently affects the serration dynamics. The size effect law is expressed as

$$\sigma = \sigma_0(1 + L/L_0)^{-1/2}(1 + ((\eta + L/L_0)(1 + L/L_0))^{-1}), \tag{3}$$

where η, L_0, and σ_0 are empirical constants determined from the experimental data. The size effect law is applicable to evaluate the deformation parameters as well as the correlated parameters in Eq. 2. The

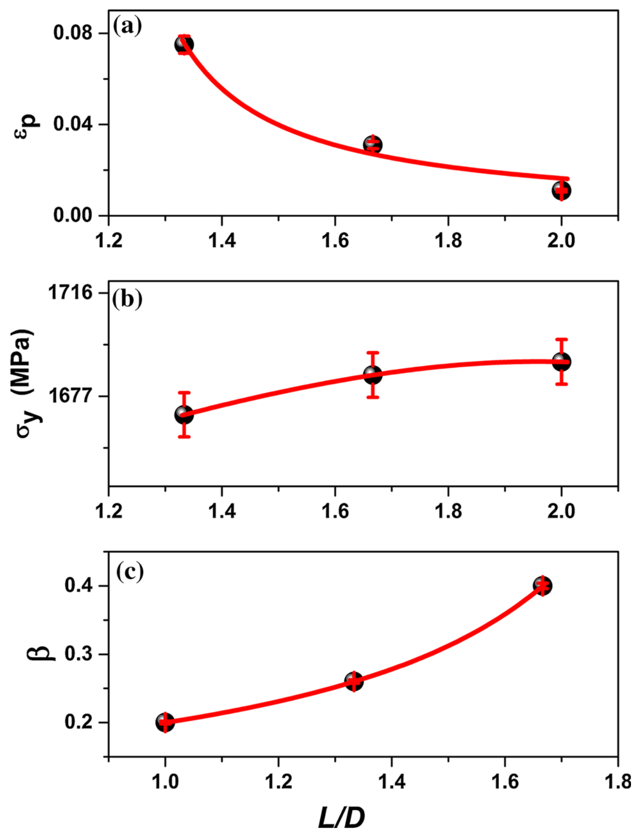

Figure 4 Size effect curves for various parameters. **a** Plastic strain ε_p. **b** Yield stress σ_y. **c** Scaling exponent β. The *red solid lines* are predictions using the size effect law, i.e., Eq. (3).

statistical distribution of the elastic energy density is calculated from the stress–strain curves. As shown in Fig. 1, the average elastic energy density is 3302, 3530, 4448, and 4932 J/m^3, corresponding to the aspect ratio of 6/3, 5/3, 4/3, and 3/3, respectively. The elastic energy density is higher with lower aspect ratio except for 6/3, which may be due to the limited serration events. With respect to the deformation-related plastic strain, yield stress, and the serration dynamics, the size effects caused by scaling exponent are shown in Fig. 4. In general, the average elastic strain energy density fits well with Eq. 3. The size effect law indicates that the serration dynamic is closely related to the aspect ratio, especially from the energy dissipation point of view.

Conclusions

In summary, the stability of serration events is affected profoundly by different aspect ratios in the plastic steady state. The SOC behavior is prone to occur and leads better ductility under lower aspect ratio, especially less than one. From energy dissipation perspective, the size effect law could predict the relation between aspect ratio and serration dynamics. The shear-band instability index reflects the aspect ratio effect on serration behavior with reasonable accuracy. The experimental analysis to the effects of aspect ratio on serration dynamics and plastic deformation could help in understanding the physical mechanisms of BMG ductility.

Acknowledgements

This work was supported by the National Natural Science Foundation of China (No.51401192, 51611130 120, 51301136, and 11572249), the Fundamental Research Funds for the Central Universities (No.310 2015ZY027 and 3102015BJ(II)JGZ019), the Aeronautical Science Foundation of China (2015ZF53072), and the Natural Science Foundation of Shaanxi Province (No.2016JM5009).

References

[1] Schuh CA, Hufnagel TC, Ramamurty U (2007) Mechanical behavior of amorphous alloys. Acta Mater 55:4067–4109

[2] Hufnagel TC, Schuh CA, Falk ML (2016) Deformation of metallic glasses: recent developments in theory, simulations, and experiments. Acta Mater 109:375–393

[3] Sun BA, Wang WH (2015) The fracture of bulk metallic glasses. Prog Mater Sci 74:211–307

[4] Qiao JW, Jia HL, Liaw PK (2016) Metallic glass matrix composites. Mater Sci Eng R 100:1–69

[5] Qiao JC, Pelletier JM (2014) Dynamic mechanical relaxation in bulk metallic glasses: a review. J Mater Sci Technol 30:523–545

[6] Sun BA, Yu HB, Jiao W, Bai HY, Zhao DQ, Wang WH (2010) Plasticity of ductile metallic glasses: a self-organized critical state. Phys Rev Lett 105:035501

[7] Ke HB, Sun BA, Liu CT, Yang Y (2014) Effect of size and base-element on the jerky flow dynamics in metallic glass. Acta Mater 63:180–190

[8] Sun BA, Pauly S, Hu J, Wang WH, Kühn U, Eckert J (2013) Origin of intermittent plastic flow and instability of shear band sliding in bulk metallic glasses. Phys Rev Lett 110:225501

[9] Antonaglia J, Wright WJ, Gu XJ, Byer RR, Hufnagel TC, LeBlanc M, Uhl JT, Dahmen KA (2014) Bulk metallic glasses deform via slip avalanches. Phys Rev Lett 112:155501

[10] Klaumünzer D, Lazarev A, Maaß R, Dalla Torre FH, Vinogradov A, Löffler JF (2011) Probing shear-band initiation in metallic glasses. Phys Rev Lett 107:185502

[11] Sun BA, Pauly S, Tan J, Stoica M, Wang WH, Kühn U, Eckert J (2012) Serrated flow and stick–slip deformation dynamics in the presence of shear-band interactions for a Zr-based metallic glass. Acta Mater 60:4160–4171

[12] Sun BA, Yang Y, Wang WH, Liu CT (2016) The critical criterion on runaway shear banding in metallic glasses. Sci Rep 6:21388

[13] Dalla Torre FH, Klaumünzer D, Maaß R, Löffler JF (2010) Stick–slip behavior of serrated flow during inhomogeneous deformation of bulk metallic glasses. Acta Mater 58:3742–3750

[14] Thurnheer P, Maaß R, Laws KJ, Pogatscher S, Löffler JF (2015) Dynamic properties of major shear bands in Zr–Cu–Al bulk metallic glasses. Acta Mater 96:428–436

[15] Qian LH, Guo PC, Meng JY, Zhang FC (2013) Unusual grain-size and strain-rate effects on the serrated flow in FeMnC twin-induced plasticity steels. J Mater Sci 48:1669–1674. doi:10.1007/s10853-012-6925-x

[16] Jiang WH, Atzmon M (2003) Rate dependence of serrated flow in a metallic glass. J Mater Res 18:755–757

[17] Lemaître A, Caroli C (2009) Rate-dependent avalanche size in athermally sheared amorphous solids. Phys Rev Lett 103:065501

[18] Ren JL, Chen C, Wang G, Mattern N, Eckert J (2011) Dynamics of serrated flow in a bulk metallic glass. AIP Adv 1:032158

[19] Wang Z, Qiao JW, Yang HJ, Liaw PK, Huang CJ, Li LF (2015) Serration dynamics in a Zr-based bulk metallic metallic glass. Metall Mater Trans A 46:2404–2414

[20] Song SX, Bei H, Wadsworth J, Nieh TG (2008) Flow serration in a Zr-based bulk metallic glass in compression at low strain rates. Intermetallics 16:813–818

[21] Yoon KS, Lee M, Fleury E, Lee JC (2010) Cryogenic temperature plasticity of a bulk amorphous alloy. Acta Mater 58:5295–5304

[22] Dalla Torre FH, Dubach AD, Nelson A, Löffler JF (2007) Temperature, strain and strain rate dependence of serrated flow in bulk metallic glasses. Mater Trans 48:1774–1780

[23] Klaumünzer D, Maaß R, Dalla Torre FH, Löffler JF (2010) Temperature-dependent shear band dynamics in a Zr-based bulk metallic glass. Appl Phys Lett 96:061901

[24] Qiao JW, Jia HL, Chuang CP, Huang EW, Wang GY, Liaw PK, Ren Y, Zhang Y (2010) Low-temperature shear banding for a Cu-based bulk-metallic glass. Scr Mater 63:871–874

[25] Qiao JW, Yang FQ, Wang GY, Liaw PK, Zhang Y (2010) Jerky-flow characteristics for a Zr-based bulk metallic glass. Scr Mater 63:1081–1084

[26] Qiao JW, Zhang Y, Liaw PK (2010) Serrated flow kinetics in a Zr-based bulk metallic glass. Intermetallics 18:2057–2064

[27] Wang Z, Qiao JW, Tian H, Sun BA, Wang BC, Xu BS, Chen MW (2015) Composition mediated serration dynamics in Zr-based bulk metallic glasses. Appl Phys Lett 107:201902

[28] Thurnheer P, Maaß R, Pogatscher S, Löffler JF (2014) Compositional dependence of shear-band dynamics in the Zr–Cu–Al bulk metallic glass system. Appl Phys Lett 104:101910

[29] Qiao JC, Yao Y, Pelletier JM, Keer LM (2016) Understanding of micro-alloying on plasticity in $Cu_{46}Zr_{47-x}Al_7Dy_x$ ($0 \leq x \leq 8$) bulk metallic glasses under compression: based on mechanical relaxations and theoretical analysis. Int J Plast 82:62–75

[30] Ren JL, Chen C, Wang G, Cheung WS, Sun BA, Mattern N, Siegmund S, Eckert J (2014) Various sizes of sliding event bursts in the plastic flow of metallic glasses based on a spatiotemporal dynamic model. J Appl Phys 116:033520

[31] Wang G, Chan KC, Xia L, Lu P, Shen J, Wang WH (2009) Self-organized intermittent plastic flow in bulk metallic glasses. Acta Mater 57:6146–6155

[32] Tong X, Wang G, Yi J, Ren JL, Pauly S, Gao YL, Zhai QJ, Mattern N, Dahmen KA, Liaw PK, Eckert J (2016) Shear avalanches in plastic deformation of a metallic glass composite. Int J Plast 77:141–155

[33] Schuh CA, Nieh TG (2003) A nanoindentation study of serrated flow in bulk metallic glasses. Acta Mater 51:87–99

[34] Golovin YI, Ivolgin VI, Khonik VA, Kitagawa K, Tyurin AI (2001) Serrated plastic flow during nanoindentation of a bulk metallic glass. Scr Mater 45:947–952

[35] Jiang WH, Fan GJ, Liu FX, Wang GY, Choo H, Liaw PK (2008) Spatiotemporally inhomogeneous plastic flow of a bulk-metallic glass. Int J Plast 24:1–16

[36] Wright WJ, Samale MW, Hufnagel TC, LeBlanc MM, Florando JN (2009) Studies of shear band velocity using spatially and temporally resolved measurements of strain during quasistatic compression of a bulk metallic glass. Acta Mater 57:4639–4648

[37] Sarmah R, Ananthakrishna G, Sun BA, Wang WH (2011) Hidden order in serrated flow of metallic glasses. Acta Mater 59:4482–4493

[38] Chen HM, Huang JC, Song SX, Nieh TG, Jang JSC (2009) Flow serration and shear-band propagation in bulk metallic glasses. Appl Phys Lett 94:141914

[39] Maaß R, Klaumünzer D, Löffler JF (2011) Propagation dynamics of individual shear bands during inhomogeneous flow in a Zr-based bulk metallic glass. Acta Mater 59:3205–3213

[40] Maaß R, Löffler JF (2015) Shear-band dynamics in metallic glasses. Adv Funct Mater 25:2353–2368

[41] Maaß R, Klaumünzer D, Villard G, Derlet PM, Löffler JF (2012) Shear-band arrest and stress overshoots during inhomogeneous flow in a metallic glass. Appl Phys Lett 100:071904

[42] Wang Z, Qiao JW, Wang G, Dahmen KA, Liaw PK, Wang ZH, Wang BC, Xu BS (2015) The mechanism of power-law scaling behavior by controlling shear bands in bulk metallic glass. Mater Sci Eng A 639:663–670

[43] Wang C, Sun BA, Wang WH, Bai HY (2016) Chaotic state to self-organized critical state transition of serrated flow dynamics during brittle-to-ductile transition in metallic glass. J Appl Phys 119:054902

[44] Hu J, Sun BA, Yang Y, Liu CT, Pauly S, Weng YX, Eckert J (2015) Intrinsic versus extrinsic effects on serrated flow of bulk metallic glasses. Intermetallics 66:31–39

[45] Wu Y, Li HX, Liu ZY, Chen GL, Lu ZP (2010) Interpreting size effects of bulk metallic glasses based on a size-independent critical energy density. Intermetallics 18:157–160

[46] Jiang WH, Liu FX, Liaw PK, Choo H (2007) Shear strain in a shear band of a bulk-metallic glass in compression. Appl Phys Lett 90:181903

[47] Han Z, Wu WF, Li Y, Wei YJ, Gao HJ (2009) An instability index of shear band for plasticity in metallic glasses. Acta Mater 57:1367–1372

[48] Bažant ZP (1984) Size effect in blunt fracture: concrete, rock, metal. J Eng Mech ASCE 110:518–535

[49] Bažant ZP, Planas J (1998) Fracture and size effect in concrete and other quasibrittle materials. CRC Press LLC, Boca Raton

[50] Wiest A, Duan G, Demetriou MD, Wiest LA, Peck A, Kaltenboeck G, Wiest B, Johnson WL (2008) Zr–Ti-based Be-bearing glasses optimized for high thermal stability and thermoplastic formability. Acta Mater 56:2625–2630

[51] Csikor FF, Motz C, Weygand D, Zaiser M, Zapperi S (2007) Dislocation avalanches, strain bursts, and the problem of plastic forming at the micrometer scale. Science 318:251–254